# Ionic transport in crystalline $SiO_2$: The role of alkali-metal ions and hydrogen impurities

P. Campone, M. Magliocco,* G. Spinolo, and A. Vedda
*Istituto Nazionale di Fisica della Materia, Dipartimento di Fisica, Universita' di Milano, Via Celoria 16, I-20133 Milano, Italy*
(Received 6 June 1995)

The ionic conductivity of synthetic quartz (both untreated and "hydrogen swept"), due to the migration of alkali-metal ions ($M^+$) dissociated from $[AlO_4\text{-}M]^0$ centers, has been investigated in an extended temperature range (550–1700 K) by impedance spectroscopy measurements. Two time-dependent effects, important for the overall interpretative framework, have been observed during high-temperature annealings: (a) during thermal treatments performed in the 900–1300 K temperature range, a monotonic enhancement of the conductivity is detected, more evident in "hydrogen swept" samples; (b) thermal treatments in the 1400–1700 K range induce a monotonic decrease of the conductivity. The interpretation of the former effect is based on the indirect role of hydrogen impurity in ionic transport, also supported by infrared spectroscopy measurements on the $[AlO_4\text{-}H]^0$ centers; the latter effect is attributed to alkali-metal ion desorption. The experimental results are interpreted in the framework of a model featuring two interacting dissociation reactions, of the $[AlO_4\text{-}M]^0$ and of the $[AlO_4\text{-}H]^0$ defects, respectively. Following this model, a satisfactory fit of the experimental data is performed, leading to the determination of the dissociation and migration energies of the alkali-metal ions as 1.19 eV and 0.25 eV, respectively.

## I. INTRODUCTION

In this paper we present a detailed study of the temperature dependence of the ac conductivity of synthetic crystalline quartz, which allows us to achieve a comprehensive view of the ionic transport in such a crystal.

Owing to the wide energy gap,[1] $SiO_2$, both crystalline and amorphous, is an excellent electric insulator. However, previous studies on electric transport properties[2–8] have demonstrated that at temperatures higher than 500 K conductivity of an ionic character occurs, due to the presence of alkali-metal ions ($M^+$) thermally freed from $[AlO_4\text{-}M]^0$ extrinsic point defects. It is interesting to note that such conductivity is highly anisotropic: in fact, along the $z$-optical axis open channels exist that favor alkali-metal migration and thus the conductivity ($\sigma$) measured with the electric field applied along this axis is very much higher than perpendicular to it.[2]

The available data in the literature mostly concern conduction in the limited range of the alpha crystallographic phase ($T<846$ K). Striking differences can be evidenced by comparing samples of different origins. Discrepancies are to be found both in the absolute values of $\sigma$, spread over more than one order of magnitude, and in the activation energies for the conductivity, varying between 0.8 and 1.4 eV.[4–6] While the variations in the absolute conductivity values can be easily interpreted in terms of different impurity concentrations, the discrepancies concerning the activation energies are puzzling. In fact, it seems that these large differences cannot be attributed to the presence of distinct charge carriers, as a useful comparison between synthetic and natural samples of different origin has shown.[4]

The interpretation of the different aspects of the phenomenology of alkali-metal transport in crystalline quartz has been treated up to now within the framework of dilute solution theory[9] applied to $[AlO_4\text{-}M]^0$ defects in the $SiO_2$ lattice. To overcome discrepancies between synthetic and natural samples, it has also been proposed that the presence of additional dissociated aluminium ions could influence the dissociation reaction of the $[AlO_4\text{-}M]^0$ center, and thus the concentration of free alkali ions, giving rise to sample-dependent conductivity curves.[4]

An important treatment that strongly influences the ionic transport properties of quartz is the "sweeping" process.[10] This process has found important uses in the fabrication of high stability quartz resonators: it consists of an electrodiffusion performed in air at high temperatures (800 K) and is effective in converting the majority of $[AlO_4\text{-}M]^0$ centers into $[AlO_4\text{-}H]^0$ defects.[11] By reducing the concentration of alkali ions, the "sweeping" treatment is effective in reducing the ionic conductivity,[6] in agreement with the fact that alkalis, and not hydrogen ions, are the charge carriers responsible for conduction. However, $[AlO_4\text{-}H]^0$ centers are found to play an interesting indirect role in the alkali transport process, as we have already shown in preliminary reports.[12,13]

We present here studies of the ionic transport of both untreated and "hydrogen swept" synthetic samples in an extended temperature range (500–1700 K). By comparing the conductivity curves of these two differently prepared crystals and by studying their dependence upon different isothermal annealings, it has been possible to give a detailed analysis of the critical role of $[AlO_4\text{-}H]^0$ defects in ionic transport. Specifically, the concentration of free alkali-metal ions is found to be governed by two interacting dissociation reactions, namely of the $[AlO_4\text{-}M]^0$ and of $[AlO_4\text{-}H]^0$ centers. This has allowed us to propose a consistent and complete interpretation of the observed phenomenology, extending previous interpretative suggestions.[4] Such an interpretation also finds support from the temperature dependence of the infrared-absorption intensity of the OH stretching modes in samples submitted to the same isothermal annealings and from recent thermally programmed desorption measurements.

## II. EXPERIMENTAL

We have studied synthetic quartz produced by Sawyer Research Products, Eastlake, Ohio: this quartz has an alu-

 

minium content of approximately 1 to 3 ppm (data supplied by Sawyer). Two varieties were examined: both the untreated Premium Quality, (PQ) quartz, and the Premium Quality "hydrogen swept" ($PQ_{sw}$). The sweeping process was performed at 500 °C in air by the supplier. In PQ samples Al impurities are mainly compensated by Na, owing to the presence of sodium carbonate in the growth process; in $PQ_{sw}$ crystals, hydrogen is the principal compensator of Al ions.

The samples studied were in the form of cylinders (diameter of 10 mm and thickness of 5 mm) with the axis parallel to the optical axis of the crystal ($z$ cut). In several measurements, up to 1000 K, thin palladium films were deposited on both faces of the sample to improve contact with the tungsten electrodes of the measurement condenser (at $T>1000$ K, Pd films were unstable).

The condenser containing the samples was heated from room temperature to 1700 K by a tungsten mesh kept in vacuum ($10^{-5}$ torr); a Pt/Pt-Rh thermocouple allowed measurement of the sample temperature with a precision of 1 K. The electrical measurements were carried out with an ac bridge (Hewlett Packard 4284a) operating in the frequency range of 20 Hz–1 MHz, with 1 V applied test-signal voltage. The electrical data were numerically analyzed on the basis of an equivalent circuit featuring a series of two parallel $RC$ elements, in order to separate the bulk parameters (resistance and capacitance) from the surface contributions. The overall sensitivity of the apparatus with respect to conductance measurements, taking into account both the sensitivity of the ac bridge and temperature-dependent leakage resistances of the measurement condenser, was evaluated to be better than $10^{-8}\ \Omega^{-1}$ up to 800 K, being reduced to approximately $10^{-7}\ \Omega^{-1}$ from 900 up to 1700 K.

Annealing treatments were performed in vacuum ($10^{-5}$ torr) from 700 to 1700 K in the same furnace used for the electrical measurements but with no electric field applied to the electrodes. The optical-absorption measurements were carried out at 80 K with a double-beam spectrophotometer (Cary 2300) in the wave-number range 3250–3600 $cm^{-1}$.

## III. RESULTS

### A. Conductivity measurements

Figure 1 shows impedance spectra of the bulk-electrode system, measured at different temperatures, in the case of PQ quartz. As already mentioned in the Experimental section, the sample and electrodes can be represented by two parallel $R$-$C$ circuits connected in series: in the complex impedance plane, each parallel $RC$ circuit is shown as a semicircle, the value of the resistance being evaluated from its intersection with the real axis. Different experimental conditions were used in order to identify the semicircle due to the bulk of the sample and to separate it from surface contributions. The spectra reported in (a) were obtained at 653 K with thin palladium layers deposited on the sample surfaces, in order to minimize the contributions due to contact resistances. Curves 1 and 2 relate to samples 5 mm and 2.5 mm thick, respectively: the bulk origin of the high-frequency arc is underlined by the dependence of the equivalent resistance on the sample thickness. In Fig. 1(b) the influence of palladium surface deposition on the low-frequency portion of the spectra is shown in the case of two measurements performed at

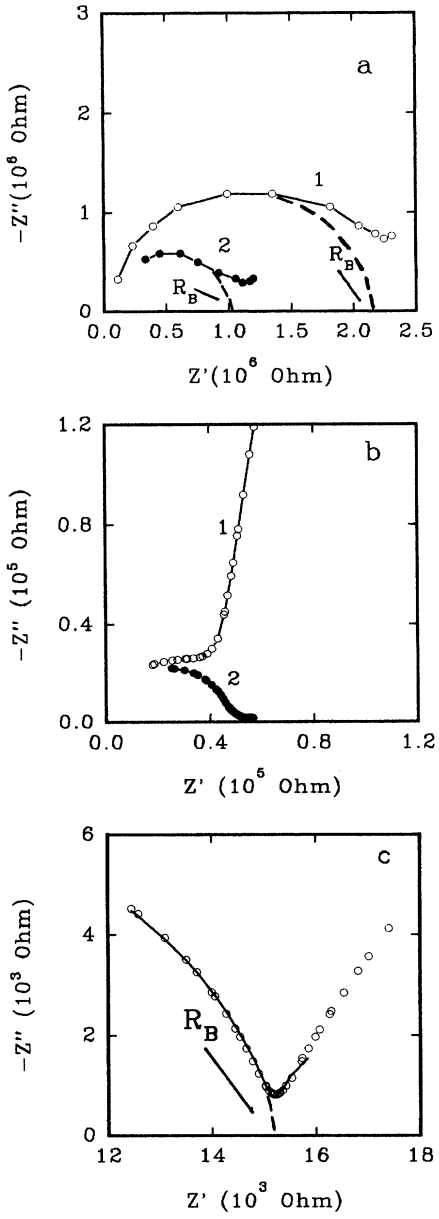


FIG. 1. Complex impedance spectra of PQ untreated quartz with the electric field oriented along the $z$-crystallographic axis recorded at different temperatures. (a) 653 K: curves 1 and 2 refer to samples with 5 and 2.5 mm thickness, respectively. Palladium coated surfaces; (b) 973 K: curve 1 was obtained with palladium coated surfaces, and curve 2 with uncoated surfaces; (c) 1370 K (uncoated surfaces).

973 K with uncoated (curve 1) and coated (curve 2) surfaces. The spectrum shown in Fig. 1(c) was obtained with uncoated surfaces ($T>1000$ K): the contribution of the electrodes is evident, nevertheless a precise evaluation of the resistance of the sample was obtainable.

Impedance spectra were measured at different temperatures from 500 to 1700 K. By taking the reciprocal of the bulk resistances, and taking into account geometrical factors, conductivity data [$\sigma(T)$] are obtained: these are reported in the Arrhenius plot of Fig. 2 both for PQ and for $PQ_{sw}$. It may

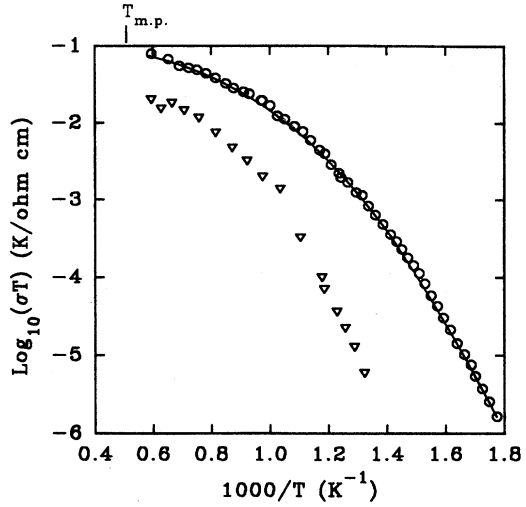


FIG. 2. Arrhenius plot of the ionic conductivity of crystalline quartz obtained with the electric field parallel to the $z$-crystallographic axis. The melting point ($T_{mp}$), at 1980 K, is also indicated. Circles, PQ; triangles, $PQ_{sw}$. Continuous line, numerical fit of the experimental data.

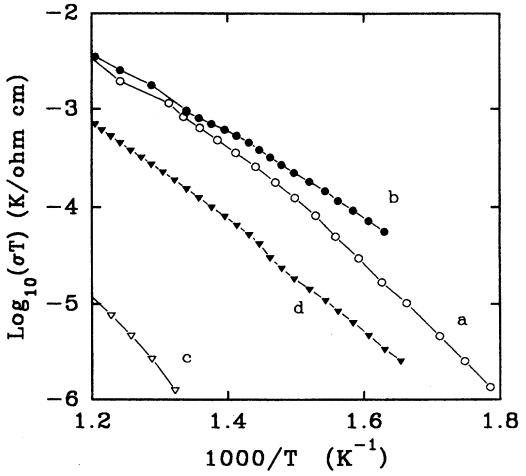


FIG. 3. Arrhenius plot of the ionic conductivity of crystalline quartz obtained with the electric field parallel to the $z$-crystallographic axis. (a) Open circles, PQ untreated sample; (b) filled circles, PQ after 10 h vacuum annealing at 1270 K; (c) open triangles, $PQ_{sw}$ untreated sample; (d) filled triangles, $PQ_{sw}$ after 10 h vacuum annealing at 1370 K.

be noted that the variation of conductivity versus temperature extends over several decades in the temperature range considered, with a monotonically decreasing slope for both samples. A considerable difference in the absolute values of the conductivity is observed, in agreement with the fact that in the $PQ_{sw}$ samples most of the alkali charge carriers have been "swept out" and substituted by hydrogen. It is interesting to note that the conductivity curve of the $PQ_{sw}$ sample also has a different shape with respect to that of the PQ specimen, being steeper in the lower temperature range.

Since we observed that $\sigma(T)$ is different in subsequent measurements, we submitted the samples to annealing treatments at different temperatures. It turned out that such annealings had a strong effect, both on the absolute values and the slope of the curves, and this will be shown and commented on below.

In Fig. 3, curves (a) and (b), we report the comparison, in the alpha crystallographic phase, between a first measurement performed on a PQ untreated sample and the same measurement repeated after the sample has been annealed for 10 h at 1270 K: a conductivity increase is evident. Hydrogen swept crystals show a similar conductivity variation but, in this case, the intensity of the phenomenon is much stronger, as shown in Fig. 3, curves (c) and (d), in the case of annealing at 1370 K. For $PQ_{sw}$ samples, the dependence of $\sigma(T)$ as a function of time at fixed temperature is quite relevant, as appears in Fig. 4. In this figure the time dependence of the conductivity at three different temperatures, up to 1100 K, is shown for three distinct, previously untreated samples. The phenomenon is more evident in the alpha crystallographic phase, where a variation of approximately a factor 4.5 is obtained after 10 h annealing. At higher temperatures, up to 1100 K, such an effect is less marked.

However, if the annealing temperature is increased above 1500 K, the opposite effect is obtained: Fig. 5 shows the conductivity variation observed during annealing at 1670 K, both in the case of PQ and $PQ_{sw}$ samples: the conductivity decreases as a function of time, being reduced by up to a factor of 2 after a 10-h treatment. Contrary to what is observed in the case of annealing performed at lower temperatures, the observed variation is similar both for PQ and $PQ_{sw}$ samples.

The complete effects of temperature treatments can thus be summarized in Fig. 6, where the conductivity curves of a $PQ_{sw}$ sample after different annealing steps (untreated, annealed at 1370 K and further annealed at 1570 K) are compared in the alpha crystallographic phase. While the first annealing at 1370 K is effective in enhancing the conductivity up to two orders of magnitude, an evident decrease is observed after the highest temperature treatment at 1570 K.

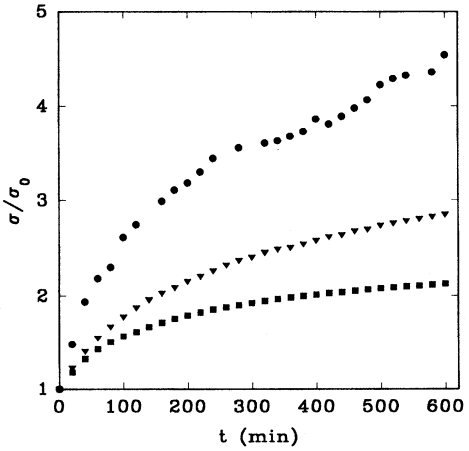


FIG. 4. Conductivity variation of $PQ_{sw}$ quartz as a function of time at different fixed temperatures. Circles, 726 K; triangles, 876 K; squares, 1075 K. The data are normalized to the initial conductivity values for each temperature.

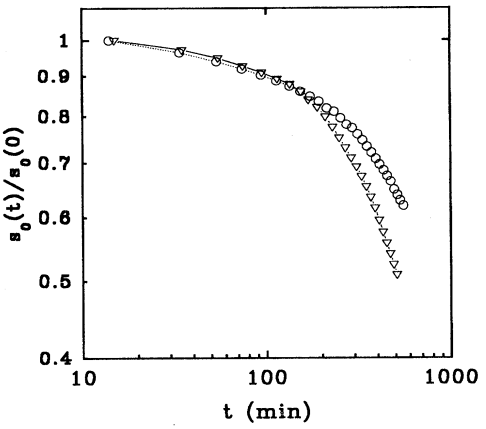


FIG. 5. Conductivity variation as a function of time recorded at 1670 K for the two types of samples considered. Circles, PQ; triangles, $PQ_{sw}$. The data are normalized to the initial values of conductivity measured after thermalization of the sample was reached.

### B. Infrared-absorption measurements

Owing to the role of hydrogen in the transport process, we also performed infrared-absorption measurements on the OH stretching vibrations,[13] here reported for completeness: the spectrum of a $PQ_{sw}$ sample, performed at 80 K, is reported in Fig. 7. The most evident structures are the $[AlO_4\text{-}H]^0$ stretching vibration at 3367 $cm^{-1}$ ("$e_2$" band), together with other OH stretching vibrations at 3396, 3435, and 3585 $cm^{-1}$ ("$s_2$", "$s_3$" and "$s_4$" bands, respectively).[11] The spectrum of a PQ sample, also reported in Fig. 7, shows only the presence of the $s$ bands, while no contribution at 3367 $cm^{-1}$ was detected. The spectra were also recorded after different thermal treatments; Fig. 8 reports the intensities of the bands as a function of annealing temperature. It may be noted that all the structures are lowered with increasing temperature, the spectrum being completely flat after annealing at 1600 K; the annealing of the "$e_2$" band is faster than that of the group of the $s$ bands.

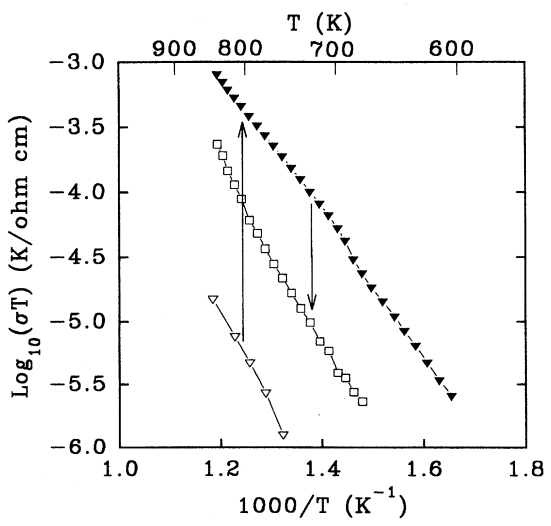


FIG. 6. Arrhenius conductivity plot of a $z$-cut $PQ_{sw}$ sample after different heat treatments. Open triangles, untreated; filled triangles, after 10 h vacuum annealing at 1370; open squares, after 10 h vacuum annealing at 1570 K.

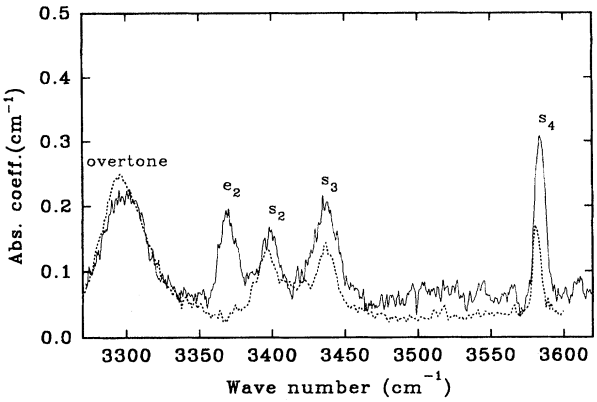


FIG. 7. Infrared-absorption spectra of crystalline quartz recorded at $T=80$ K. Continuous line, $PQ_{sw}$; dashed line, PQ.

## IV. DISCUSSION

The attribution of the ionic conductivity of crystalline $SiO_2$ to the migration of alkali-metal ions dissociated from aluminium centers is generally accepted; this picture is also supported by different experimental evidences such as dielectric loss measurements[14] and infrared-absorption studies,[15] which demonstrate the predominant role of aluminium and alkali-metal impurities with respect to other extrinsic (or possibly intrinsic) defects in the transport phenomenology.

However, although the hydrogen content of the samples considered here is relevant for transport phenomenology, particularly as far as $PQ_{sw}$ crystals are concerned, our results

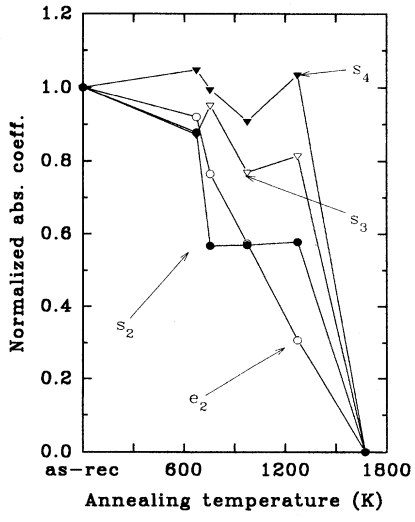


FIG. 8. Intensities of the infrared-absorption bands of $PQ_{sw}$ quartz as a function of 10 h annealing treatments at different temperatures. The spectra are recorded at 80 K. The intensities are normalized with respect to the values relative to the untreated sample.

lead us to conclude that a direct contribution of this impurity to transport, as a charge carrier, is to be excluded. The comparison between PQ and $PQ_{sw}$ samples shows that the latter, hydrogen rich, have much lower conductivity values.

A few considerations are possible in order to justify the lack of a direct contribution of hydrogen ions to transport: the activation energy of this impurity could be significantly higher with respect to the corresponding values of alkali ions; alternatively, free charged hydrogen ions could be unstable in the $SiO_2$ lattice and lead to the formation of molecules; in this respect preliminary observations have indeed demonstrated that $H_2$ molecules are detected in the desorption spectrum of crystalline $SiO_2$, above 500 K.[16]

The experimental results presented above, namely the comparison between conductivity curves of untreated and hydrogen swept crystals and the effect of annealings up to 1300 K both in conductivity and infrared absorption, suggest the occurrence of a strong interaction between $[AlO_4\text{-}H]^0$ and $[AlO_4\text{-}M]^0$ centers. Thus, although hydrogen impurities do not play a direct role in the ionic transport of this material, nevertheless an indirect influence of this species on the alkali-metal transport can be inferred.

In the following we shall propose a conductivity model, in which the concentration of alkali-metal ions is derived by taking into account two coupled dissociation reactions, of $[AlO_4\text{-}M]^0$ and of $[AlO_4\text{-}H]^0$ defects. These two dissociation reactions can be written as

$$[AlO_4\text{-}M]^0 \leftarrow\!\rightarrow [AlO_4]^- + [M]^+, \tag{1a}$$

$$[AlO_4\text{-}H]^0 \leftarrow\!\rightarrow [AlO_4]^- + [H]^+. \tag{1b}$$

In equilibrium, the following two mass-action laws hold:

$$\frac{[AlO_4]^-[M]^+}{[AlO_4\text{-}M^+]^0} = K_1(T) = Z_M^{-1} \exp(-E_D^M/k_BT), \tag{2a}$$

$$\frac{[AlO_4]^-[H]^+}{[AlO_4\text{-}H^+]^0} = K_2(T) = Z_H^{-1} \exp(-E_D^H/k_BT), \tag{2b}$$

where $E_D^M$ and $E_D^H$ are the dissociation energies of the $[AlO_4\text{-}M^+]^0$ and the $[AlO_4\text{-}H^+]^0$ centers, respectively, $k_b$ is the Boltzmann constant, $Z_M$ and $Z_H$ are the numbers of equivalent orientations of the pairs.[17]

By defining $m$ as the atomic fraction, relative to silicon atoms, of dissociated $[AlO_4\text{-}M^+]^0$ centers (also corresponding to the atomic fraction of $M^+$ ions) and $m_0$ as the total atomic fraction of $[AlO_4\text{-}M^+]^0$ centers prior to dissociation, and by using similar definitions for the $[AlO_4\text{-}H^+]^0$ centers, the atomic fraction of $[AlO_4]^-$ defects at a given temperature can be written as $(m+h)$, while the atomic fractions of associated $[AlO_4\text{-}M^+]^0$ and $[AlO_4\text{-}H^+]^0$ centers are $(m_0-m)$ and $(h_0-h)$, respectively. With these definitions, Eq. (2a) and (2b) can be written as

$$m(m+h) = Z_M^{-1}(m_0-m)\exp(-E_D^M/k_BT), \tag{3a}$$

$$h(m+h) = Z_H^{-1}(h_0-h)\exp(-E_D^H/k_BT). \tag{3b}$$

By combining Eqs. (3a) and (3b), a third-order equation is obtained, whose solution gives the atomic fraction, $m$, of $M^+$ ions:

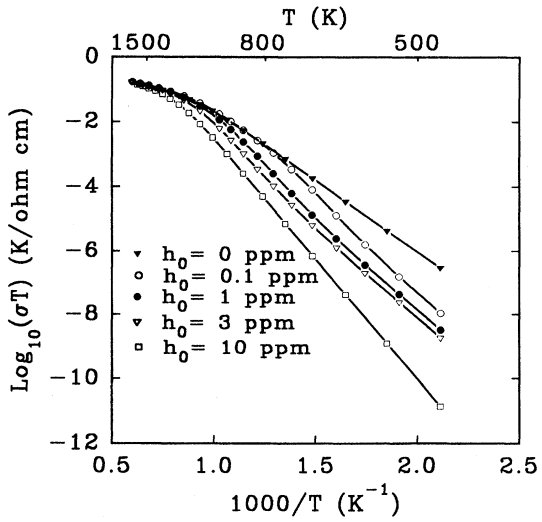


FIG. 9. Computer simulations of $\sigma T$ vs $1/T$ derived from Eqs. (4)–(6) for different $h_0$ values. Other parameters are kept fixed: $E_D^M$=1.22 eV, $E_D^H$=0.3 eV, $m_0$=2 ppm, $E_m$=0.27 eV, $\nu=10^{13}$ sec$^{-1}$.

$$(E-F)m^3 + (E^2 - EF - Em_0 - Fh_0)m^2 + (EFm_0 - 2E^2m_0)m + m_0^2E^2 = 0. \tag{4}$$

The terms $E$ and $F$ are defined here as $E = Z_M^{-1}\exp(-E_M^D/kT)$ and $F = Z_H^{-1}\exp(-E_H^D/kT)$.

The atomic fraction $m$ so obtained enters into the classical ionic conductivity expression:

$$\sigma = mNe\mu, \tag{5}$$

where $N$ is the number per unit volume of silicon atoms, $e$ is the electric charge, and the mobility $\mu$ is defined as

$$\mu = \mu_0 \exp(-E_m/k_bT) = \frac{er^2\nu}{k_bT}\exp(-E_M/k_bT). \tag{6}$$

In this equation $e$ is the electric charge, $r$ is the jump distance, $\nu$ is the oscillation frequency, and $E_M$ the migration energy of the alkali-metal ion.

In order to verify the dependence of the conductivity upon the different parameters $E_D^M$, $E_D^H$, $E_m$, $m_0$, $h_0$, and $\mu_0$ within the framework of this model, a number of computer simulations have been performed. Of particular significance is the variation of conductivity as a function of $[AlO_4\text{-}H]^0$ concentration, $h_0$, shown in the set of curves of Fig. 9, where the other parameters are kept fixed. A strong enhancement of the conductivity curve is observed as a function of the lowering of the concentration of $[AlO_4\text{-}H]^0$ centers, particularly in the alpha crystallographic phase; it is to be noted that this general behavior is not dependent upon the specific choice of the other parameters. In this context, the strong conductivity enhancement observed after heat treatments (shown in Fig. 3), can be interpreted as the consequence of the lowering of $[AlO_4\text{-}H]^0$ defects. This interpretation is also confirmed by direct measurements of the intensity of the IR stretching vibration band of the $[AlO_4\text{-}H]^0$ centers as a function of annealing treatments, as illustrated in Fig. 8.

Let us now spend a few words on the details of the analysis of our experimental results on the basis of Eq. (5). We have numerically solved Eq. (4) by using Newton's method, the atomic fraction of alkali-metal ions $m(T)$ being obtained as a function of four parameters: $m_0$, $h_0$, $E_D^M$, and $E_D^H$. Then, numerical interpolations of the experimental curves, such as those reported in Fig. 2, were performed on the basis of Eq. (5), for PQ samples; the measurements performed on $PQ_{sw}$ specimens were not suitable for these fits owing to their strong time dependence. Due to the number of free parameters involved, satisfactory evaluations were difficult to attain in the complete temperature range. However, particularly in the beta and trydymite crystallographic phases, a simplified equation for the $m$ parameter, derived from (3a) under the assumption of complete dissociation of the $[AlO_4\text{-}H]^0$ centers ($h=h_0$) was found to reproduce correctly the experimental data:

$$m=-\frac{h_0+Z_M^{-1}E}{2}+\left[\left(\frac{h_0+Z_M^{-1}E}{2}\right)^2+Z_M^{-1}m_0E\right]^{1/2}. \quad (7)$$

In this case, considering that the $[AlO_4\text{-}M]^0$ center has two equivalent orientations ($Z_M=2$),[14] reasonable values for the parameters concerning the alkali-metal charge carriers were obtained: $E_D^M=1.19$ eV $\pm 0.06$ eV, and $E_m=0.25$ eV $\pm 0.03$ eV were found; the frequency $\nu$ turned out to be of the order of $10^{13}$ $sec^{-1}$ if a jump distance of the order of 1 Å was considered. A numerical fit is reported in Fig. 2. We remark that the value of $E_D^M$ is consistent with data in the previous literature.[4] Moreover, in the past evaluations of the alkali-metal migration energy, $E_m$, have also been made on the basis of radiation-induced conductivity (RIC) measurements on both synthetic and natural samples.[2,4,6,8] These led to somewhat controversial and sample-dependent results, with energy values ranging from 0.14 to 0.45 eV; particularly in natural samples the migration process also appeared to be governed by the presence of additional shallow traps contributing to a modification of the activation energy. In fact, our evaluation appears to be consistent with the majority of the RIC measurements performed on the synthetic quartzes.

A few comments should now be made on the high-temperature ($T>1500$ K) annealing effect, for which the interpretation is not strictly related to the model discussed above. In this case, as illustrated in Fig. 5, the lowering of the conductivity as a function of time is approximately similar in both the PQ and $PQ_{sw}$ samples, demonstrating that the different compensation of the Al centers is of lesser importance. Our first proposal is that, at very high temperatures, alkali-metal desorption from the sample may also occur, leading to a lowering of the charge-carrier concentration. Such desorption should be possible, as well as that occurring during the "sweeping out" process, the only difference being that here the driving force is not a dc field but a concentration gradient.

All the data presented here relate to ionic transport parallel to the $z$ crystallographic axis. An effort to extend the experiments to transport perpendicular to the $z$ axis in quartz and on synthetic amorphous silica is under way.

## V. CONCLUSIONS

In the present paper we believe to have given complete experimental data on ionic transport parallel to the $z$ axis in synthetic quartz, including thermal annealing effects on the $\sigma(T)$ and parallel effects on OH concentration. We have proposed a picture of the transport process that, through consideration of the mass-action law applied to the $[AlO_4\text{-}M]^0$ and $[AlO_4\text{-}H]^0$ centers, justifies the shape of $\sigma(T)$ and its dependence on the annealing treatments. Such a picture allows an evaluation of the dissociation and migration energies of alkalis in quartz; the values obtained appear to be compatible with previously existing data.

The disappearance of absorption related to the OH stretching vibrations after high-temperature treatments enters the general picture as well. Our work provides the possibility to obtain a deeper insight into the influence of "hydrogen sweeping" in the conductivity of quartz.

## ACKNOWLEDGMENTS

It is our pleasure to acknowledge fruitful discussions with our colleagues M. Martini and A. Paleari. We are also grateful to Professor A. Miotello for stimulating discussions and for a private communication on the desorption measurements performed by his group.

*Present address: Siemens Telecomunicazioni SpA, S. S. Padana Superiore, I-20060 Cassina de' Pecchi (Mi), Italy.

[1] C. Bosio and W. Czaja, Philos. Mag. B **63**, 7 (1991).
[2] R. C. Hughes, Radiat. Eff. **26**, 225 (1975).
[3] T. M. Glushkova and M. M. Firsova, Sov. Phys. Crystallog. **12**, 871 (1968).
[4] H. Jain and A. S. Nowick, J. Appl. Phys. **53**, 477 (1982).
[5] J. Toulouse, E. R. Green, and A. S. Nowick, Proc. 37th Ann. Freq. Control Symp. USAERADCOM, 125 (1983).
[6] E. R. Green, J. Toulouse, J. Wacks, and A. S. Nowick, Proc. 38th Ann. Freq. Control Symp. IEEE, 32 (1984).
[7] S. Lazzari, M. Martini, A. Paleari, G. Spinolo, A. Vedda, Nucl. Instrum. Methods Phys. Res. Sect. B **32**, 299 (1988).
[8] M. Martini, A. Paleari, G. Spinolo, and A. Vedda, J. Phys. Condens. Matter **2**, 6921 (1990).
[9] A. B. Lidiard, Handb. Phys. **20**, 246 (1957).
[10] J. J. Martin, IEEE Trans. Ultrason. Ferroelec. Freq. Control **35**, 288 (1988).
[11] L. E. Halliburton, N. Koumvakalis, M. E. Markes, and J. J. Martin, J. Appl. Phys. **52**, 3565 (1981).
[12] A. Cascella, M. Magliocco, G. Spinolo, and A. Vedda, in *Proceedings of the XII International Conference on Defects in Insulating Materials*, edited by O. Kanert and J. M. Spaeth (World Scientific, Singapore, 1993), p. 920.
[13] P. Campone, M. Magliocco, G. Spinolo, and A. Vedda, Radiat. Eff. Defects Solids (to be published).
[14] D. S. Park and A. S. Nowick, Phys. Status Solidi A **26**, 617 (1974).
[15] A. Kats, Philips Res. Rep. **17**, 133 (1962).
[16] A. Miotello (private communication).
[17] R. G. Fuller, in *Point Defects in Solids*, edited by J. H. Crawford and S. L. Slifkin (Plenum, New York, 1972), p. 103.